Acta Pharmaceutica Sinica B 2020;10(5):913–927

Chinese Pharmaceutical Association
Institute of Materia Medica, Chinese Academy of Medical Sciences

Acta Pharmaceutica Sinica B

www.elsevier.com/locate/apsb
www.sciencedirect.com

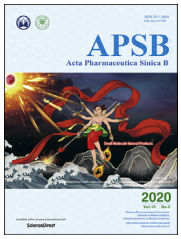

ORIGINAL ARTICLE

Self-assembled small molecule natural product gel for drug delivery: a breakthrough in new application of small molecule natural products

Kangkang Zhi[†], **Jiacheng Wang**[†], **Haitian Zhao**, **Xin Yang**[*]

School of Chemistry and Chemical Engineering, Harbin Institute of Technology, Harbin 150000, China

Received 25 June 2019; received in revised form 18 August 2019; accepted 22 September 2019

KEY WORDS

Natural products;
Gels;
Self-assembly;
Drug delivery;
Antitumor

Abstract Natural products, as a gift of nature to humanity, have long been used as drugs or pharmacological actives to help people cure various diseases. Yet we still know comparatively little about their ability to be materials. In recent years, some small molecule natural products isolated from traditional Chinese medicines have been found to have new features, namely, self-assembly to form gels (*i.e.*, natural product gels, NPG). However, the application development of these natural products is seriously lacking, which greatly weakens their practical value and delays the maturity of the field. Here, a series of self-assembled triterpenoid natural products are used as materials (gel scaffolds) to construct drug delivery systems. Surprisingly, these NPG not only exhibit the excellent self-healing, controlled gelation, good safety and sustained release, but also achieve synergistic treatment of tumors through bioactive natural products. Compared with non-bioactive gel scaffolds, NPG scaffolds show great advantages in tumor therapy, including optimal tumor inhibition, preferable health, better body recovery, stronger immune function, less toxic side effects and longer survival. The successful construction of NPG scaffolds not only takes full advantage of the self-assembled natural products, but also takes an important step in the development of new applications for natural products.

*Corresponding author. Tel.: +86 451 86403309; fax: +86 451 86403379.
E-mail address: yangxin@hit.edu.cn (Xin Yang).
[†]These authors made equal contributions to this work.

Peer review under responsibility of Institute of Materia Medica, Chinese Academy of Medical Sciences and Chinese Pharmaceutical Association.

https://doi.org/10.1016/j.apsb.2019.09.009

1. Introduction

Natural products, as a gift of nature to humanity, are widely used in drugs, foods and cosmetics due to their interesting pharmacological activity, good biocompatibility and health care functions[1−3]. The importance of natural products in these fields has led to extensive research into their isolation, purification, synthesis and biological activity. Yet to date we still know comparatively little about their ability to self-assemble to form materials. Recently, triterpenoids, steroids, glycosides, peptides, and anthraquinones of small molecule natural products with self-assembly ability isolated from traditional Chinese medicines have been discovered one after another[4−9]. These natural products can form a soft matter, natural product gels (NPG), by self-assembly with a solvent. As an emerging field, the current research on such natural products mainly focuses on the discovery of new NPGs and the biological activity of NPGs (or NPG) itself before and after self-assembly[5,8]. However, there are still few developments in its application, and the only applications are also the use of synthetic template as nanomaterials[10] and *in vitro* encapsulation studies[11]. In these applications, the advantages of natural products are not maximized and are not revealed, which greatly weakens the practical value of self-assembled natural products and delays the maturity of the field.

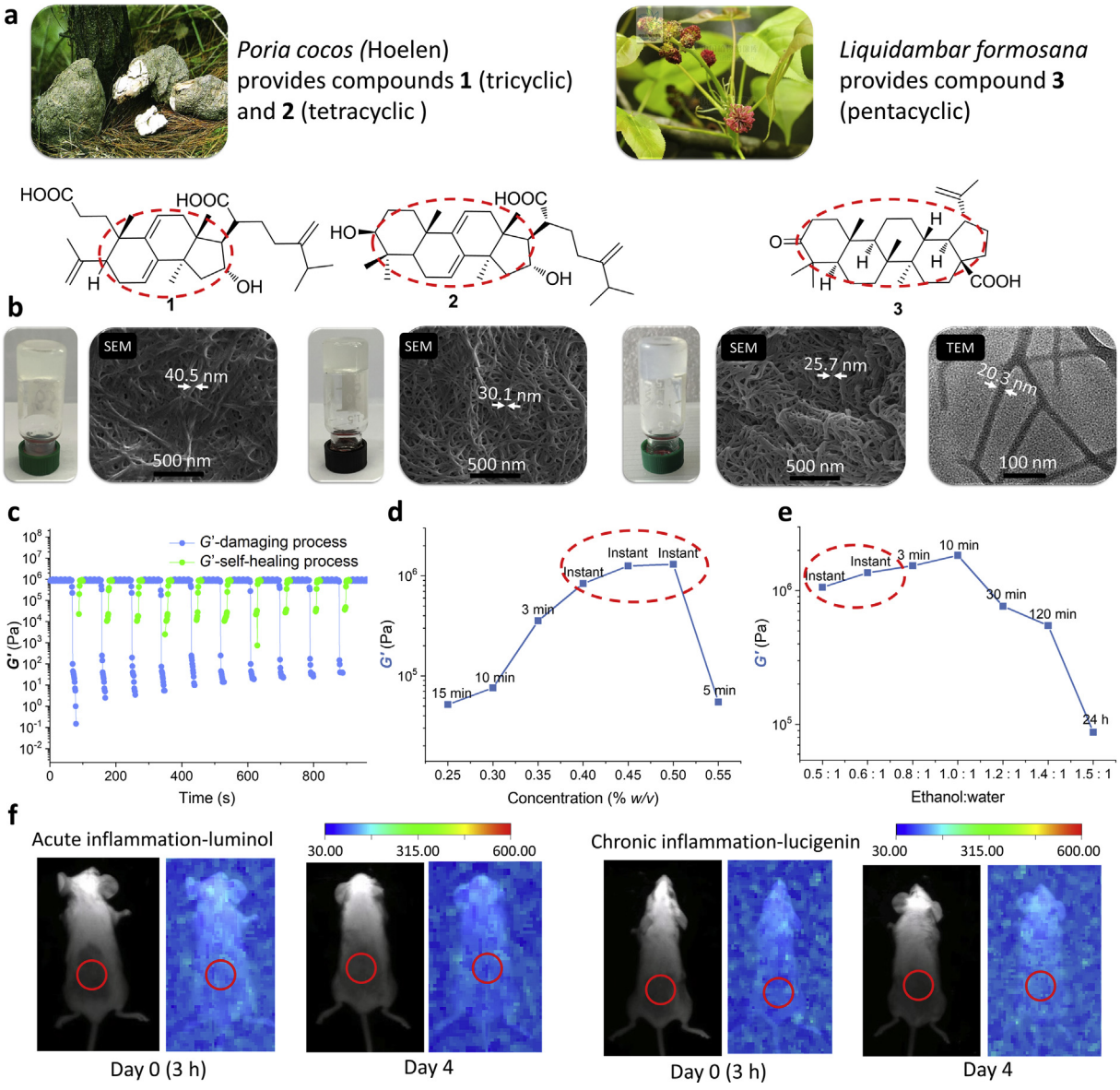

Figure 1 Construction of injectable NPG scaffolds. (a) Photograph of *Poria cocos* and *Liquidambar formosana*, and structures of compounds **1**−**3**. (b) The **1**−**3**/NPG (at 1.6%, 1.0%, 0.25% *w/v*, respectively. ethanol:water = 1:1) and their micromorphology (including SEM and TEM). (c) Self-healing of **3**/NPG (ten destruction-recovery cycles of **3**/NPG, 0.4% *w/v*, ethanol:water = 1:1). (d) Controlled gelation and mechanical properties of **3**/NPG at varying gelator concentrations, ethanol:water = 1:1. (e) Controlled gelation and mechanical properties of **3**/NPG at varying ratio of ethanol to water, 0.8% *w/v*). (f) Implant safety of **3**/NPG (red circle corresponds to the injection site, multi-wavelength data on black background, luminescence data on blue background).

Gel, as an intelligent soft material, has been studied extensively as a scaffolds for drug delivery in the biomedical field[12−14]. In particular, injectable gel scaffolds receive more attention because they can directly enter the lesion to treat the disease[15−17]. However, even designed injectable gel scaffolds with optimal gel characteristics by synthesis are not bioactive[12]. Inspired by the advantages of natural products, we can imagine that the gel scaffolds constructed with self-assembled natural products will inherently have low toxicity, good biocompatibility, biodegradability and biological activity. As such, for the applications development of self-assembled natural products, the construction of injectable NPG scaffolds for drug delivery becomes the first choice. As one of the most abundant terpenoids in nature, triterpenoid natural products have a variety of important biological activities and pharmacological effects, and have always received the attention of researchers[18]. However, the current research on self-assembled triterpenoid NPG matrix has only *in vitro* drug encapsulation and release[6,7,11], and more in-depth research has not been explored.

Here, we develop a series of injectable gel scaffolds constructed with self-assembled natural products of triterpenoids with a tricyclic to pentacyclic skeleton structure (compounds **1**−**3**, Fig. 1a). Tumors were selected as model diseases to validate their efficacy in drug delivery. These NPGs not only exhibit the excellent self-healing, controlled gelation, good safety and sustained release, but also achieve synergistic treatment of tumors through bioactive natural products. Compared with non-bioactive gel scaffolds, injectable NPG scaffolds show great advantages in tumor therapy (encompassing optimal tumor inhibition, preferable health, better body recovery, stronger immune function, less toxic side effects and longer survival). The successful construction of injectable NPG scaffolds not only takes full advantage of the natural products, compensates for the lack of biological activity of injectable gel scaffolds, but also provides a new paradigm for exploring the practical application of self-assembled natural products.

2. Materials and methods

2.1. Reagents and animals

Ibuprofen (>98%) and lipopolysaccharides (LPS, derived from *Escherichia coli* 055: B5) were purchased from Sigma−Aldrich (Saint Louis, MO, USA). Luminol (98%) and lucigenin (95%) were purchased from J&K Scientific (Beijing, China). Doxorubicin HCl (>98%) and paclitaxel (>99%) were purchased from Dalian Meilun Biotechnology Co., Ltd (Dalian, China). MTT (98%) was purchased from Alfa Aesar (Heysham, UK). *p*-Xylene (99%) was purchased from Honeywell Fluka (Morristown, NJ, USA). Unless otherwise stated, the above reagents were used as received without further purification. All solvents were purchased from Tianjin Kemiou Chemical Reagent Co., Ltd (Tianjin, China).

Poria cocos (Schw.) Wolf and *Liquidambar formosana* were purchased from Sankesong herbal medicine market, which were identified by Prof. Zhenyu Wang who majored in Chinese medicine classification, School of Chemistry and Chemical Engineering, Harbin Institute of Technology, Harbin, China. The voucher specimens (Nos. 201454 and 201464) are deposited at the School of Chemistry and Chemical Engineering, Harbin Institute of Technology, China.

The KM mice (male, 20 ± 2 g) and BALB/c mice (female, 20 ± 1 g) were purchased from Harbin Medical University and maintained in accordance with the Guidelines for Animal Care and Use of Laboratory Animals, following protocols approved by the Institutional Animal Care and Use Committee (IACUC) at the Harbin Medical University, China.

2.2. General information

Scanning electron microscopy images of gels were recorded on a Quanta 200FEG SEM spectrometer at 20 kV, 10 mA, SE mode and spot size 3.5 (Hillsboro, OR, USA). Prior to observation, the xerogel was sputter coated with a thin layer of gold. Transmission electron microscopy images of the gels were recorded on a Tecnai G2 20 TWIN transmission electron microscope (Hillsboro) with the support being a copper mesh. The rheology measurements were performed using a Kinexus pro + Rheometer (Malvern, UK), equipped with a temperature controller and parallel stainless steel plates (20 mm diameter, 0.5 mm gap). The gel after shaking was placed in the shearing gap of the rheometer and was allowed to incubate at 15 °C. Subsequently it was submitted to a frequency sweep or stress sweep experiment. To minimize solvent evaporation, a liquid trap device was placed over the sample chamber. The 1D NMR experiments were performed on a Bruker DRX-400 (Rheinstetten, Germany) at 400 MHz. UV−Vis spectra was obtained on a TU-1900 PERSEE spectrometer (Beijing, China). IR spectra was recorded on a PerkinElmer Spectrum FT-IR spectrophotometer (Waltham, MA, USA) as KBr pellets and the absorption frequencies were expressed in reciprocal centimeters (cm^{-1}). Mass spectral studies were carried out on a Hewlett−Packard 5989B MS (ESI) (Palo Alto, CA, USA). Silica gel (Qingdao, China), reversed phase silica gel (Kyoto, Japan), sephadex LH-20 (Boston, MA, USA) were used for column chromatography. TLC was performed on silica gel GF254 and was visualized with UV light (254 nm).

2.3. Extraction, isolation and identification of compounds *1*−*3*

Compounds **1** and **2**: the air-dried powder of the fruiting body of *Poria cocos* (6 kg) was extracted with 95% (*v*/*v*) ethanol (1:8, × 2) in a water bath to obtain the crude extract, which was suspended in water. The suspension was then partitioned with chloroform (1:1, × 3) to afford the chloroform extract. The chloroform extract was subjected to vacuum pressure liquid chromatography on a D101 macroporous resin column (EtOH/H_2O, 0%−100%) to yield 7 fractions (Frs. 1−7). Gel-active testing confirmed that the gelled fraction was present in the Frs. 3 and 6. Fr. 3 was further chromatographed on a silica gel column eluted with a gradient of CH_2Cl_2/MeOH (0%−100%) to afford 3 fractions (Frs. 3a−c). Fr. 3a was separated by Sephadex LH-20 column eluted with $CHCl_3$/MeOH (1:1) to yield compound **1** (4.1 g). The Fr. 6 was further chromatographed on a silica gel column eluted with a gradient of CH_2Cl_2/MeOH (0%−100%) to afford 5 fractions (Frs. 6a−e). Fr. 6b was then repeatedly purified by chromatography on a reverse-phase C18 column (MeOH/H_2O, 0%−100%), a Sephadex LH-20 column ($CHCl_3$/MeOH, 1:1) to give compound **2** (2.1 g).

Compound **1** was obtained as a white amorphous; powder purity, 97.94% (HPLC); HRESIMS *m*/*z* 521.3251 (Calcd. 521.3237) $[M+Na]^+$ ($C_{31}H_{46}O_5$). The IR spectrum displayed absorption bands for hydroxyl (at 3288 cm^{-1}), carbonyl (at 1708 cm^{-1}) and vinyl (at 1643 cm^{-1}). ^1H NMR (C_5D_5N, 400 MHz) δ 5.35 (1H, s, H-11), 5.30 (1H, s, H-7), 4.99 (1H, s, H-

31a), 4.86 (1H, s, H-31b), 4.84 (1H, s, H-28a), 4.78 (1H, s, H-28b), 4.53 (1H, dd, H-16), 2.95 (1H, dd, H-20), 2.86 (1H, dd, H-17), 1.75, 1.51, 1.11, 1.04, 1.00, 0.99 (6 × $-CH_3$); ^{13}C NMR (C_5D_5N, 100 MHz) δ 36.19 (C-1), 30.03 (C-2), 176.46 (C-3), 149.10 (C-4), 50.58 (C-5), 28.39 (C-6), 117.80 (C-7), 141.66 (C-8), 137.31 (C-9), 38.65 (C-10), 120.11 (C-11), 36.80 (C-12), 45.44 (C-13), 49.13 (C-14), 43.63 (C-15), 76.24 (C-16), 57.43 (C-17), 48.27 (C-20), 178.47 (C-21), 31.18 (C-22), 33.04 (C-23), 155.85 (C-24), 33.90 (C-25), 21.85 (C-26), 21.69 (C-27), 112.00 (C-28), 22.09 (C-29), 24.67 (C-30), 106.87 (C-31). Compound **1** was identified as poricoic acid A by comparison of its spectroscopic data with this reported in the literature[19].

Compound **2** was obtained as a white amorphous powder, purity 96.20% (HPLC), EIMS *m/z* 484 $[M]^+$ ($C_{31}H_{48}O_4$). The IR spectrum displayed absorption bands for carbonyl (at 1708 cm^{-1}) and vinyl (at 1640 cm^{-1}). ^1H NMR (C_5D_5N, 400 MHz) δ 5.64 (1H, d, H-7), 5.40 (1H, d, H-11), 4.99 (1H, s, H-31a), 4.85 (1H, s, H-31b), 4.54 (1H, dd, H-16), 3.46 (1H, dd, H-3), 2.95 (1H, m, H-20), 1.51, 1.22, 1.13, 1.08 (× 2), 1.01, 1.00 (7 × $-CH_3$). ^{13}C NMR (C_5D_5N, 100 MHz) δ 36.26 (C-1), 28.62 (C-2), 78.00 (C-3), 39.29 (C-4), 49.79 (C-5), 23.48 (C-6), 121.22 (C-7), 142.70 (C-8), 146.37 (C-9), 37.84 (C-10), 116.50 (C-11), 36.26 (C-12), 45.07 (C-13), 49.36 (C-14), 44.39 (C-15), 76.41 (C-16), 57.56 (C-17), 17.6 (C-18), 22.95 (C-19), 48.46 (C-20), 178.56 (C-21), 31.40 (C-22), 33.15 (C-23), 156.01 (C-24), 34.09 (C-25), 21.97 (C-26), 21.84 (C-27), 28.78 (C-28), 16.58 (C-29), 26.56 (C-30), 107.00 (C-31). Compound **2** was identified as dehydrotumulosic acid by comparison of its spectroscopic data with the literature[20].

Compound **3**: the air-dried powder of the infructescence of *L. formosana* (5 kg) was extracted with 95% (*v/v*) ethanol (1:6, × 2) in a water bath to obtain the crude extract, which was suspended in water. The suspension was then partitioned with chloroform (1:1, × 3) to afford the chloroform extract. The chloroform extract was subjected to silica gel column chromatography eluting with a gradient of petroleum ether/acetone (100:0 → 0:100, *v/v*) to afford 7 fractions (Frs. 1−7). Gel-active testing confirmed that the gelled fraction was present in the Fr. 2. The Fr. 2 was further vacuum chromatographed on a silica gel column eluted with a gradient of hexane/ethyl acetate (100:0 → 0:100, *v/v*) to afford 3 fractions (Frs. 2a−c). Gel test showed that the Fr. 2a had gel-activity and was then repeatedly purified by chromatography on a silica gel column (hexane/acetone, 100:0 → 0:100, *v/v*), a sephadex LH-20 column ($CHCl_3$/MeOH, 1:1) and reverse-phase C18 column (MeOH/H_2O, 0%−100%) to give compound **3** (3.0 g).

Compound **3** was obtained as white amorphous powder, purity 96.3% (HPLC). HRESIMS *m/z* 477.3354 (Calcd. 477.3339) $[M+Na]^+$ ($C_{30}H_{46}O_3$). The IR spectrum displayed absorption bands for carbonyl (at 1701.41 cm^{-1}), carboxyl (at 1687.15 cm^{-1}) and vinyl (at 3067.16 and 1641.11 cm^{-1}). ^1H NMR (CD_3Cl, 400 MHz) δ 4.73 (1H, s, H-29a), 4.60 (1H, s, H-29b), 3.00 (1H, m, H-19), 1.68, 1.06, 1.00, 0.98, 0.96, 0.91 (6 × $-CH_3$). ^{13}C NMR (CD_3Cl, 100 MHz) δ 39.7 (C-1), 34.2 (C-2), 218.3 (C-3), 47.5 (C-4), 55.1 (C-5), 19.8 (C-6), 33.7 (C-7), 40.8 (C-8), 50.0 (C-9), 37.1 (C-10), 21.5 (C-11), 25.6 (C-12), 38.7 (C-13), 42.6 (C-14), 30.7 (C-15), 32.2 (C-16), 56.6 (C-17), 49.4 (C-18), 47.0 (C-19), 150.4 (C-20), 29.8 (C-21), 37.2 (C-22), 26.8 (C-23), 21.1 (C-24), 16.1 (C-25), 16.0 (C-26), 14.8 (C-27), 182.7 (C-28), 110.0 (C-29), 19.5 (C-30). Compound **3** was identified as liquidambaric acid by comparison of its spectroscopic data with the literature[21].

2.4. *Preparation of **1−3**/NPG and drug-loaded **3**/NPG*

Preparation of **1−3**/NPG: in a container, the compound is first dissolved in ethanol and then a certain amount of water is added. The resulting mixture was shaken well and allowed to stand. When the container could be inverted without change of shape of its content, that is, the gel is formed. All samples concentrations were expressed in % as the ratio of gelator weight (mg) to liquid volume (mL). Ethanol and water mixtures were expressed as volume ratios (ethanol/water = 1:1).

Preparation of drug-loaded **3**/NPG: similar to the method of NPG preparation, the difference is that for the hydrophilic drug doxorubicin hydrochloride (DOX), the added water becomes an aqueous solution of DOX, and for the hydrophobic drug antitumor drug paclitaxel (PTX), the ethanol not only dissolves the compound **3** but also dissolves the PTX.

The drug loading of DOX and PTX was set to 4 mg/mL during the experiment to meet the self-healing ability, injectability of drug-**3**/NPG as well as the drug content required for cancer treatment.

2.5. *Evaluation of acute and chronic inflammation for **1−3**/NPG*

The assay was carried out according to the process by Tseng's et al[22]. First, BALB/c mice were anesthetized with 2% isoflurane in the induction chamber. The NPG equal to the drug-loaded NPG dose were injected subcutaneously into the back of the anesthetized mice (n = 3). When the mice were under anesthesia, the mice were injected intraperitoneally with 200 μL of luminol solution (10 mg/mL, dissolved in saline) or 100 μL of lucigenin solution (2.5 mg/mL, dissolved in saline), respectively, and then returned to the squirrel cage. At the desired time, the mice were anesthetized with a 2% isoflurane-mixed gas, and then transferred to an imaging chamber of a bioluminescence imaging system (Carestream FX pro, Kodak, Rochester, NY, USA) to monitor the bioluminescence of the mice.

2.6. *Anti-inflammatory activity of compounds **1−3***

The *in vitro* anti-inflammatory activity assay was performed according to the method modified by Cho et al[23]. The mouse macrophages RAW264.7 was obtained from Cell Resource Center, Shanghai Institutes for Biological Sciences, CAS, China. Cell culture reagents were obtained from Invitrogen (New York, NY, USA). RAW264.7 cells were grown in DMEM media containing 10% fetal bovine serum and 100 IU/mL penicillin and 100 μg/mL streptomycin. All cells were grown at 37 °C in 5% CO_2 atmosphere. The RAW264.7 cells were planted into 96-well plate at 4.0×10^5 cells per well in 100 μL of media and incubated at 37 °C for 12 h. The LPS and the various concentrations of compounds samples were then added to the wells for 24 h. The supernatant was then collected and assayed for TNF-α content using commercially available kits according to the manufacturer's instructions (Nanjing Jiancheng Bioengineering Institute-TNF-α assay kit, Nanjing, China). All experiments were repeated at least six times.

The *in vivo* anti-inflammatory activity assay was carried out according to the process modified by Vogel et al[24]. KM mice (male, 20±2g) were randomly divided into 11 groups (6 in each group). The group includes: group 1: model (glycerol-gelatin

vehicle). Group 2: ibuprofen. Group 3: **1**-loaded glycerol-gelatin (0.5 mg per mouse). Group 4: **1**-loaded glycerol-gelatin (1.0 mg per mouse). Group 5: **1**-loaded glycerol-gelatin (2.0 mg per mouse). Group 6: **2**-loaded glycerol-gelatin (0.5 mg per mouse). Group 7: **2**-loaded glycerol-gelatin (1.0 mg per mouse). Group 8: **2**-loaded glycerol-gelatin (2.0 mg per mouse). Group 9: **3**-loaded glycerol-gelatin (0.5 mg per mouse). Group 10: **3**-loaded glycerol-gelatin (1.0 mg per mouse). Group 11: **3**-loaded glycerol-gelatin (2.0 mg per mouse). Glycerol-gelatin vehicle is prepared by mixing glycerol/water/gelatin in a ratio of (50:50:3), magnetically stirring at 60 °C for 30 min, and then cooling to room temperature. Drug-loaded glycerol-gelatin is prepared by mixing a certain amount of the drug with the glycerol-gelatin vehicle, magnetically stirring at 60 °C for 30 min, and then cooling to room temperature. First, the both sides of the right ears of mice received 80 μL of *p*-xylene by topical application. Half an hour after xylene applied to the right ears of mice, the mice in group 1 were treated with vehicle of glycerol-gelatin on both sides of the left and right ear as model groups. The mice in the other groups were treated with the corresponding sample on both sides of the left and right ear. Half an hour after application of the sample, the mice were sacrificed and 7 mm punches were made in the left and the right ear by the borer. Circular sections of both ears were weighed and the differences in weights of the left and right ear discs of mice were recorded as edema degree. The anti-inflammatory activity was evaluated in accordance with the following Eq. (1):

$$\text{Inhibition}\ (\%) = 1 - \frac{E_t}{E_c} \times 100 \quad (1)$$

where E_t is the average edema of the treated group and E_c is the average edema of the model group.

2.7. Release of drug from drug-loaded 3/NPG

The *in vitro* release of the drug from the drug-loaded **3**/NPG was carried out under sink conditions with respect to DOX and PTX, using a CNP dissolution apparatus DT-6 (Tianjin, China) (Basket Method) at 100 rpm and 37 °C, in different release media. After the desired time, 3 mL of release medium was filtered through a 0.45 μm filtering membrane. The released DOX was analyzed by UV−Vis spectroscopy. The released PTX was analyzed by HPLC. The cumulative release rate (E) was calculated as follows Eq. (2):

$$E\ (\%) = \frac{V_0 C_n + V_e \sum_1^{n-1} C_{n-1}}{M_0} \times 100 \quad (2)$$

where E (%) is the drug release percentage. V_0 (mL) is the total volume of release medium. C_n (mg/mL) is the drug concentration at the nth time. V_e (mL) is the volume of each sample. M_0 (mg) is the total amount of drug. All experiments were carried out in sextuplicate. Analysis conditions: UV detection wavelength 480 nm. The standard curve for DOX in the range of 0.215−13.750 μg/mL is $y = 38.307x+0.111$ and the correlation coefficient R^2 is 0.999. Analysis conditions and standard curve of PTX: the Agilent 1100 series HPLC (Santa Clara, CA, USA). Chromatographic column: TC-C18 Analytical 4.6 mm × 250 mm, 5 μm column. Mobile phase: acetonitrile/water = 65:35. UV detector wavelength: 227 nm. Column temperature: 25 °C. Flow rate: 1 mL/min. Injection volume: 20 μL. The standard curve for PTX in the range of 66.0−781.3 ng/mL is $y = 0.0364x+0.0411$ and the correlation coefficient R^2 is 0.999.

The *in vivo* storage and release of DOX-**3**/NPG were carried out in BALB/c mice bearing 4T1 tumors ($n = 3$), with a mixed solution of ethanol and water of DOX not containing compound **3** (DOX-EW) as a control. The DOX-**3**/NPG and DOX-EW were injected intratumorally into BALB/c mice bearing 4T1 tumors, respectively, and mice were sacrificed at 1 h, 1, 2, and 7 day after i.t. administration to collect tumors and main organs. Tumors and main organs were analyzed using a multi-spectral *in vivo* imaging system (Carestream FX pro, Kodak). A rough quantification of DOX was performed by an *in vivo* imaging system using the mean intensity of the DOX fluorescence signal. Quantification of DOX was performed by measuring the DOX amount in the tumor by HPLC. Briefly, the tumors were homogenized in saline (1 g tissue/5 mL saline). Seven volumes of extraction solution containing methanol and ethyl acetate (2:5, *v*/*v*) were subsequently added. The resulting mixture was vortexed for 3 min, and the organic and aqueous phases were separated by centrifugation at 10,000 rpm for 10 min using TDZ4A-WS centrifuge (Changsha, China). The organic phase was collected and dried under nitrogen. The extract was dissolved in 1.5 mL of distilled water and 20 μL aliquots were used for HPLC analysis. Analysis conditions: the Agilent 1100 series HPLC. Chromatographic column: TC-C18 Analytical 4.6 mm × 250 mm, 5 μm column. Mobile phase: acetonitrile/water (containing 1‰ acetic acid) = 25:75. FLD detector: excitation 254 nm, emission 557 nm. Column temperature: 25 °C. Flow rate: 1 mL/min. Injection volume: 20 μL. The standard curve for DOX in the range of 0.125−2.5 μg/mL is $y = 0.0947x+3.0252$ and the correlation coefficient R^2 is 0.996, and in the range of 2.5−40.0 μg/mL is $y = 0.3364x+0.0783$ and the correlation coefficient R^2 is 0.997.

2.8. In vitro antitumor activity of drug-loaded 3/NPG

The 4T1 murine breast cancer cells and MCF-7 human breast cancer cells were obtained from Cell Resource Center, Shanghai Institutes for Biological Sciences, CAS, China. Cell culture reagents were obtained from Invitrogen. The 4T1 cells were grown in DMEM media containing 10% fetal bovine serum and 100 IU/mL penicillin and 100 μg/mL streptomycin. MCF-7 cells were grown in RPMI 1640 media containing 10% fetal bovine serum and 100 IU/mL penicillin and 100 μg/mL streptomycin. All cells were grown at 37 °C in 5% CO_2 atmosphere. Cell viability was evaluated by a standard MTT (3-(4,5-dimethyl-2-thiazolyl)-2,5-diphenyl-2*H*-tetrazoliubromide) assay. The cancer cells were planted into 96-well plate at 4.0×10^5 cells per well in 100 μL of media and incubated at 37 °C for 12 h. Then, the incubation medium was removed, and compound **3**, free DOX, DOX-loaded **3**/NPG, free PTX or PTX-loaded **3**/NPG in 200 μL of media with various concentrations was added. The cells without the coincubation with sample were used as a control. The cells were subjected to MTT assays after being incubated for another 24 h. The absorbance of the solution was measured at 570 nm on a Bio-Rad 680 microplate reader (Hercules, CA, USA). The cell viability (%) was calculated according to Eq. (3):

$$\text{Cell viability}\ (\%) = \frac{A_{\text{sample}}}{A_{\text{control}}} \times 100 \quad (3)$$

where A_{sample} and A_{control} are the absorbance values of the test samples at 570 nm, respectively. All experiments were repeated at least six times.

2.9. *In vivo experiment of DOX-loaded 3/NPG*

Solid tumor model of 4T1 tumor cell were established in BALB/c mice by subcutaneously inoculation of 4×10^4 tumor cells on the right flank of the mice. The BALB/c mice bearing 4T1 tumors were randomly divided into 10 groups (16 in each group, 8 of which were used to evaluate the therapeutic effect of different formulations on tumors except survival time, and the remaining 8 were only used to evaluate survival time), and treated with the corresponding sample when the tumor volume reached 300−350 mm^3. Ten treatment groups were evaluated in the experiment, including (1) DOX-**3**/NPG (i.t.); (2) DOX-loaded glycerol-gelatin, DOX-GG (i.t.), as a control for the anti-inflammatory active **3**/NPG scaffold; (3) **3**/NPG vehicle control, **3**/NPG (i.t.); (4) glycerol-gelatin vehicle control, GG (i.t.); (5) DOX ethanol/water solution, DOX-EW (i.t.), as a control for the non-gel scaffold; (6) ethanol/water mixed solvent vehicle control, EW (i.t.); (7) DOX saline solution-one injection, DOX (i.v. one), as a control for different administration; (8) DOX saline solution-daily injection, DOX (i.v. daily), as a control for different administration; (9) saline blank control, saline (i.t.); (10) **3**-loaded glycerol-gelatin, **3**-GG (i.t.), as a group for studying the antitumor activity of compound **3** alone. In the above experiment, the total amount of DOX was set to 25 mg/kg per mouse and the injection volume of all treatment groups was 125 μL. In addition, non-tumor-bearing BALB/c mice fed under the same conditions were reared as reference for normal mice (normal group).

Tumor volume of tumor-bearing mice was measured at intervals of one day after treatment. Tumor volumes were calculated based on the length and width of the tumor by Eq. (4):

$$V = \left[\left(\text{Length} \times \text{width}^2\right) / 2\right] \quad (4)$$

The mice were euthanized at the end of the treatments, and the tumor, heart, spleen and blood of the mice were collected to evaluate the therapeutic effect. Tumors of the mice were analyzed by H&E staining for cell necrosis and TUNEL staining for cell apoptosis. Inflammatory factors and related enzymes in the blood of mice were determined using commercially available kits according to the manufacturer's instructions, including serum levels of myeloperoxidase (MPO, Nanjing Jiancheng Bioengineering Institute-MPO Assay Kit) and plasma levels of prostaglandin E_2 (PGE_2, Cusabio Biotech-Mouse PGE_2 ELISA Kit, Houston, TX, USA).

The mice were bled blood through the ocular vein and the routine blood tests of blood samples was measured by BC-2800 Auto Hematology Analyzer (Mindray, Shenzhen, China) on days 0, 7, and 14 after treatment. Body weight of tumor-bearing mice were measured at intervals of one day after treatment to assess the body recovery. The superoxide dismutase (SOD) were determined using commercially available kits according to the manufacturer's instructions (Nanjing Jiancheng Bioengineering Institute-SOD Assay Kit) to assess the body's ability to recover. The spleens of mice were weighed in order to evaluate immune function. Heart of the mice was analyzed by H&E staining for heart damage. The survival of the mice was monitored daily after administration.

2.10. *Statistical analysis*

Statistical analyses were performed with the GraphPad Prism 5 (GraphPad Software). Multiple groups were compared using one-way ANOVA. Two groups were compared using *t*-test. *P* values of less than 0.05, 0.01 and 0.001 were considered statistically significant, very significant and extremely significant, respectively. Data are presented as means ± SD.

3. Results and discussion

3.1. *Construction of injectable NPG scaffold*

Triterpenoid natural product (compounds **1**−**3**) having a tricyclic to pentacyclic skeleton structure were selected as subjects (Fig. 1a). Among them, compounds **2** (dehydrotumulosic acid) and **3** (liquidambaric acid) are newly discovered NPGs from *P. cocos* and *L. formosana* by the method we established previously[4]. Briefly, the powders of dried traditional Chinese medicine are extracted with organic solvents, and the gel ability of the extract was determined. The crude extract having gel ability is then isolated by various chromatographic techniques (including silica gel, reverse-phase C18, sephadex LH-20) under the guidance of gel-activity to yield compounds **2** and **3**. Compound **1** (poricoic acid A) is the first NPG we discovered[4]. The three of them have the following characteristics: 1) each of them can self-assemble with a good biocompatible ethanol-water mixed solvent to form a supramolecular gel under mild conditions (Fig. 1b), providing an important basis for its direct clinical application. This is critical because most synthetic gelators typically only gel in organic solvents, and the toxicity of organic solvents limits their use in drug delivery. 2) The tricyclic to pentacyclic structure of compounds **1**−**3** cover the main structure of triterpenoids (Fig. 1a), and studying them thus helps us understand the potential of triterpenoid NPG in drug delivery. 3) Compounds **1**−**3** have previously been extensively studied as pharmacologically active ingredients (including antitumor, antiviral activity, anti-inflammatory, induce apoptosis, etc.)[25−28]. These interesting pharmacological activities are very beneficial for their use in the treatment of diseases.

Compounds **1**−**3** can easily form a gel (**1**/NPG, **2**/NPG, **3**/NPG, respectively, Fig. 1b) by incorporation. That is, the compound is dissolved in ethanol, and then a certain amount of water is added. Stability test showed that these gels can be stored for at least one year under sealed conditions. Morphological observations revealed that the gels formed by different skeleton compounds are composed of regular nanoscale self-assembled fibers (20−40 nm in diameter) (Fig. 1b). Such structures are flexible and dynamic and facilitates encapsulation of the drug[29]. The test results of the critical gelation concentration (CGC) showed that the **3**/NPG had the smallest CGC (0.25% *w*/*v*), that is, it has an optimum gel ability (**1**/NPG and **2**/NPG are 1.6% and 1.0%, respectively). It is very likely that by incorporation, the smallest polar compound **3** precipitate first in the polar solvent (ethanol−water mixed solvent) upon gel formation, and compound **3** is thus more likely to form a gel at a low concentration. Calculating the $\log P_{oct/wat}$ value (partition coefficient) of compounds **1**−**3** also supports this view (results are 5.635, 7.637, 8.075, respectively)[30].

Thixotropy and self-healing properties were investigated as prerequisites for the construction of injectable gels. The thixotropy research showed that by shaking the gel and then standing still, all NPG can return to the original gel state within a certain period of time, indicating that they all have thixotropic properties. The self-healing properties of **1**−**3**/NPG were investigated by a rheometer. Taking **3**/NPG as an example, the **3**/NPG can

quickly return to its original state in more than 10 destruction−recovery cycles, suggesting excellent self-healing properties (Fig. 1c). It is worth mentioning that, unlike the gel of the single solvent system, **1**−**3**/NPG are composed of two-solvent system. Thus, the regulation of gel self-healing time and mechanical properties can be achieved by changing not only the gelatos concentration but also the ratio of ethanol to water, which provides greater flexibility in the regulation of the gel system. Also taking **3**/NPG as an example, by varying the different gel compositions, the self-healing time of **3**/NPG can be controlled in an instant to 24 h (Fig. 1d and e), which achieves controlled gelation. At the same time, the mechanical properties of **3**/NPG can also be adjusted by one order of magnitude (Fig. 1d and e), that is, the storage modulus (G') can be regulated between 10^5 and 10^6 Pa, which indicates good controllable mechanical properties of **3**/NPG. The **1**/NPG and **2**/NPG can also achieve the above excellent performance regulation by reasonable changes in gel composition.

Injectability, which is not available for most gels, is the most basic and most critical property in the construction of injectable gel scaffolds. The injectability test results of **1**−**3**/NPG revealed that all three NPGs have excellent injectability, that is, **1**−**3**/NPG were able to be ejected from the medical syringe in a homogeneous state and can instantly recover the gel state (Supporting Information Movie S1).

As an implantable gel scaffold, its safety must be considered before *in vivo* experiments. In the safety evaluation, the inflammation produced by the implanted scaffold is the main tissue reaction and excessive inflammation can result in the scaffold not being used clinically. Therefore, we evaluated the implant safety of **1**−**3**/NPG by animal models of acute and chronic inflammation based on bioluminescence[12,22]. Taking **3**/NPG as an example, we first injected **3**/NPG subcutaneously in the back of the anesthetized mice (Fig. 1f). Luminol and lucigenin are injected then intraperitoneously into anesthetized mice, which are known to react with reactive oxygen species produced at the site of inflammation to produce bioluminescence and are used as indicators of acute and chronic inflammation, respectively. After that, we recorded the bioluminescence of the mice at different times after the injection. The results showed that no bioluminescence signal was detected in either the model of acute (3 h) or chronic (day 4) inflammation (Fig. 1f), indicating good safety of **3**/NPG.

The above results indicated that injectable gel scaffolds constructed from triterpenoid natural products exhibit long-lasting stability, good thixotropic properties, excellent self-healing properties, controlled gelation and mechanical properties and safety, demonstrating that the injectable NPG scaffolds have the prerequisites for *in vivo* application.

3.2. *Formation of injectable NPG scaffold*

The NPG formation is explored through a variety of spectral techniques. By analyzing the structures of the compounds **1**−**3**, it is known that their molecular structures can be divided into three parts, namely, alkane polycyclic skeleton moieties (such as tricyclic, tetracyclic, and pentacyclic), olefin moieties (such as double bonds) and an oxygen-containing moieties (such as a hydroxyl group). For the potential interactions generated by different structural moieties, we selected 2D NMR NOESY (for van der Waals force), UV (for $\pi-\pi$ interaction), IR (for hydrogen bonding) and 1D ^{1}H NMR (for hydrogen bonding) to study them.

The 2D NMR NOESY spectrum based on the NOE effect can provide correlation between nuclei physically close to each other (typically 4.5 Å or less), regardless of whether there is a covalent bond between them[31,32]. The 2D NOESY spectrum of compound **3** in a mixed solvent of deuterated ethanol and deuterated water (4:1) at different concentrations was tested as an example. The results showed that in 6 mg/mL (the solution state) (Supporting Information Fig. S1a)and 12 mg/mL (near but below CGC) (Fig. 2a-left), only a few correlation peaks were recorded and all peaks appeared in the upfield (circled in red in Fig. 2a-left). However, at 15 mg/mL (CGC), most of the hydrogen nuclei on the pentacyclic skeleton of compound **3** showed correlation peaks from the upfield to the downfield (Fig. 2a-right), indicating that the distance between the compound **3** molecules became more closer (less than 4.5 Å) when the gel was formed (that is, after self-assembly). We calculated the molecular length of compound **3** to be 13.068 Å (Fig. 2b), so the approximate van der Waals radius (r_w) of the compound **3** molecule was 6.534 Å. The distance of the 2D NOESY spectrum showing the correlation peak signal (less than 4.5 Å) is much smaller than the r_w (6.534 Å) of compound **3** molecule, that is, the van der Waals force occurs between the compound **3**, and mainly exists in the form of repulsive force. In order to rule out the correlation peak in the above 2D NOESY spectrum being caused by the excessive concentration of compound **3**, we also tested the 2D NOESY spectrum of compound **3** in non-gel solvent deuterated chloroform (*i.e.*, no self-assembly occurs) at the same concentration (15 mg/mL) and under supersaturation conditions. The results showed that only a few correlation peaks appear in the upfield of the NOESY spectrum both at the same concentration and supersaturation (Fig. S1b), which is similar to the case where the compound **3** does not self-assemble at low concentrations in the mixed solvent of deuterated ethanol and deuterated water. This ruled out false positive results and demonstrated the contribution of van der Waals forces to the formation of **3**/NPG.

The UV spectrum of compound **3** at various concentrations was determined to obtain the potential role of the double bond in the structure of the compound **3**. The absorption peaks near 210 and 280 nm in the UV spectrum are attributed to the $\pi-\pi^*$ transition of their olefinic double bonds (C═C) and the $n-\pi^*$ transition of their carbonyl double bonds (C═O), respectively (Fig. 2c). As the concentration increases, the absorption peak of C═O only shows a change in peak height; while the absorption peak of C═C not only increases the peak height, but also causes a significant redshift. This suggests that only the C═C exerts its $\pi-\pi$ interaction in the formation of **3**/NPG.

The IR spectra of compound **3** obtained from non-gel solvent (chloroform) and gel solvent (ethanol water mixed solvent) were determined to explore the formation of hydrogen bonds of oxygen-containing moieties. The results shows that the absorption peak of ketone carbonyl (C═O) of compound **3** is red shifted from the non-gel state of 1709 cm^{-1} to the gel state of 1702 cm^{-1}, revealing the existence of hydrogen bonds (Fig. 2d). In addition, we also tested ^{1}H NMR of compound **3** at different concentrations to further confirm the formation of hydrogen bonds. However, since the carboxyl hydrogen as the active hydrogen undergoes rapid exchange in the protic solvent (mixed solvent of deuterated ethanol and deuterated water), it cannot be detected. This makes it impossible to judge the formation of hydrogen bonds by the change in the chemical shift of the carboxyl hydrogen. Interestingly, we observed changes of the hydrogen proton signal in ^{1}H

NMR of compound **3**! This phenomenon not only confirms the formation of hydrogen bonds, but also serves as an important evidence for participation of solvent in the formation of **3**/NPG. In ^{1}H NMR of compound **3**, as the concentration increased (from 6 to 12 mg/mL), the broad single peak at 4.63 ppm moved to the downfield (at 4.83 ppm), revealing that the hydrogen bond was enhanced (Fig. 2e and Supporting Information Fig. S2). This peak is determined as the peak of water proton in the mixed solvent by the assignment of the hydrogen proton signal. It is known that water may exchange protons with other exchangeable protons to form a single peak, and the chemical shift of the single peak appears at the average position after interaction with the exchange proton[31]. The exchangeable protons in compound **3** have only carboxyl protons, so the enhancement of hydrogen bonds of solvent can be considered to indirectly reflect the enhancement of hydrogen bonds of carboxyl. This indicates that hydrogen bonds provides support for the formation of **3**/NPG. Moreover, when the concentration of compound **3** was continuously increased to the CGC (15 mg/mL), the ^{1}H NMR spectrum showed that the chemical shift of the broad single peak was unchanged, but the peak width was narrowed (Fig. 2e). This narrowing of the peak width indicates that the exchange rate of water protons and carboxyl protons becomes faster in the process of gradually forming **3**/NPG. This reflects the fact that the solvent is also involved in the formation of **3**/NPG. The possible cause of this phenomenon is that with self-assembly to a certain stage (when chemical shift is unchanged), the formed ordered self-assemblies are structurally better exchangeable with the solvent, and thus having a faster exchange rate (peak narrowing).

The above results demonstrate that the formation of NPG is not only supported by weak non-covalent forces (including van der Waals forces occurring between the skeleton moieties compound, $\pi-\pi$ interactions of olefin moieties and hydrogen bonds of oxygen-containing moieties), but also by the participation of solvents.

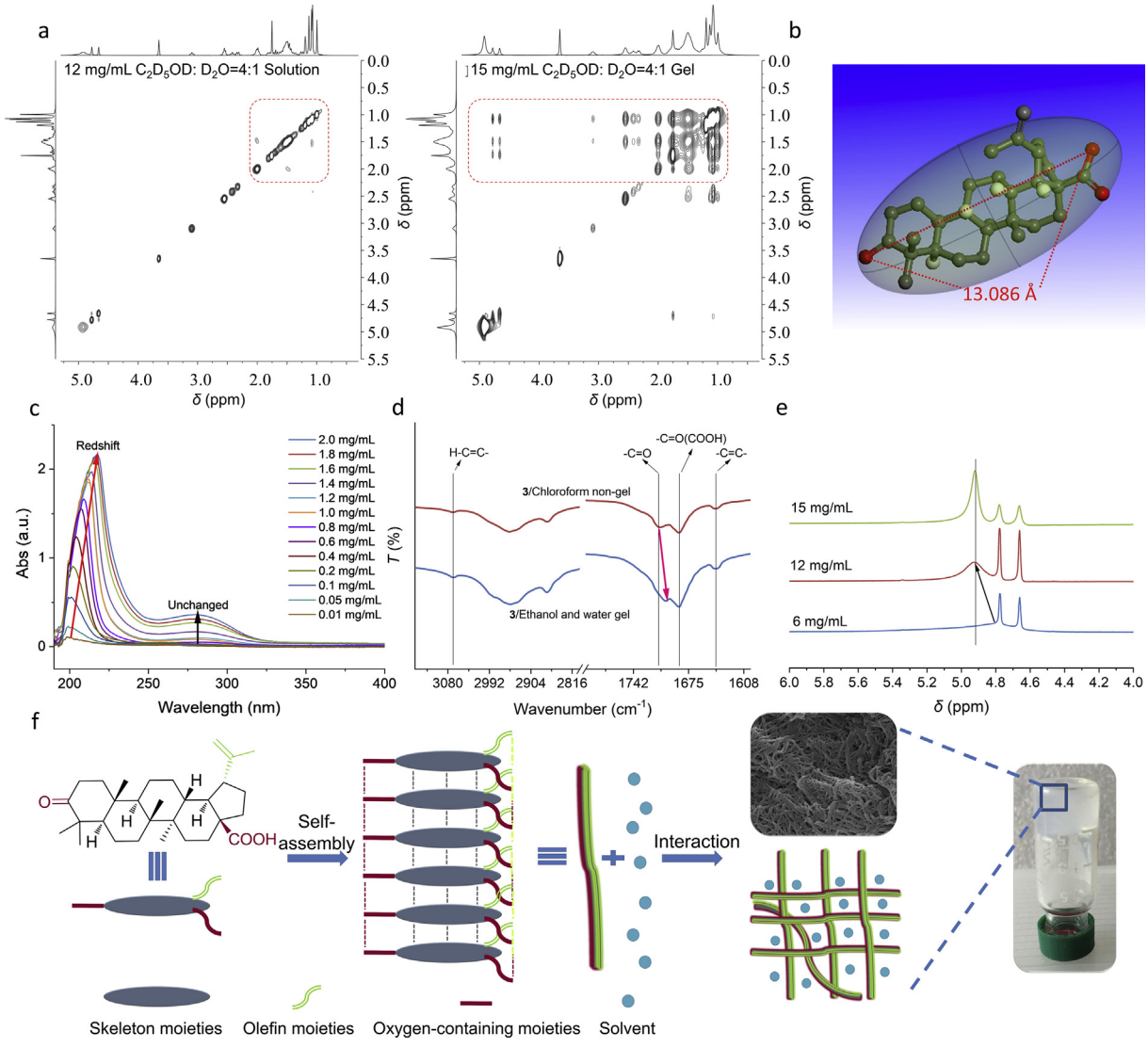

Figure 2 Formation of injectable NPG scaffold. (a) 2D NOESY spectra of compound **3** in mixed solvent of deuterated ethanol and deuterated water (4:1) at different concentrations. (b) Molecular length of compound **3**. (c) UV spectra of compound **3** in ethanol/water mixed solvent (1:1) at different concentrations. (d) IR spectra of compound **3** obtained from non-gel and gel. (e) ^{1}H NMR spectra of compound **3** in mixed solvent of deuterated ethanol and deuterated water (4:1) at different concentrations. (f) A possible self-assembly formation process of NPG.

Based on this, a possible self-assembly formation process of NPG is proposed (Fig. 2f). Self-assembled compounds first self-assemble to form one−dimensional fibers through three different non-covalent interactions, and then these one−dimensional fibers gradually form a NPG having a three−dimensional network fiber structure under interaction with a solvent.

3.3. *Validation of injectable NPG scaffold effectiveness*

To validate the efficacy of NPG scaffold for drug delivery in the treatment of disease *in vivo*, the tumor was selected as a model disease. Based on the fact that inflammation is closely related to the development of tumors and inhibition of inflammation can effectively improve the therapeutic effect[33,34], the compounds with optimal anti-inflammatory activity in compounds **1**−**3** are screened and used to construct NPG scaffolds for tumor treatment.

3.3.1. *Determination of anti-inflammatory activity of compounds **1**−**3***

The *in vitro* anti-inflammatory activity of compounds **1**−**3** was evaluated by measuring TNF-α released from lipopolysaccharide-stimulated mouse macrophages (RAW264.7)[23]. As a major pathophysiological mediators in inflammatory diseases, TNF-α can be used to evaluate the anti-inflammatory activity of compounds *in vitro*[35]. The *in vitro* anti-inflammatory results showed that the IC_{50} values of compounds **1**−**3** against TNF-α were 160.16, 366.77, and 84.19 μmol/L, respectively (Supporting Information Table S1), that is, compound **3** had the strongest anti-inflammatory effect *in vitro*.

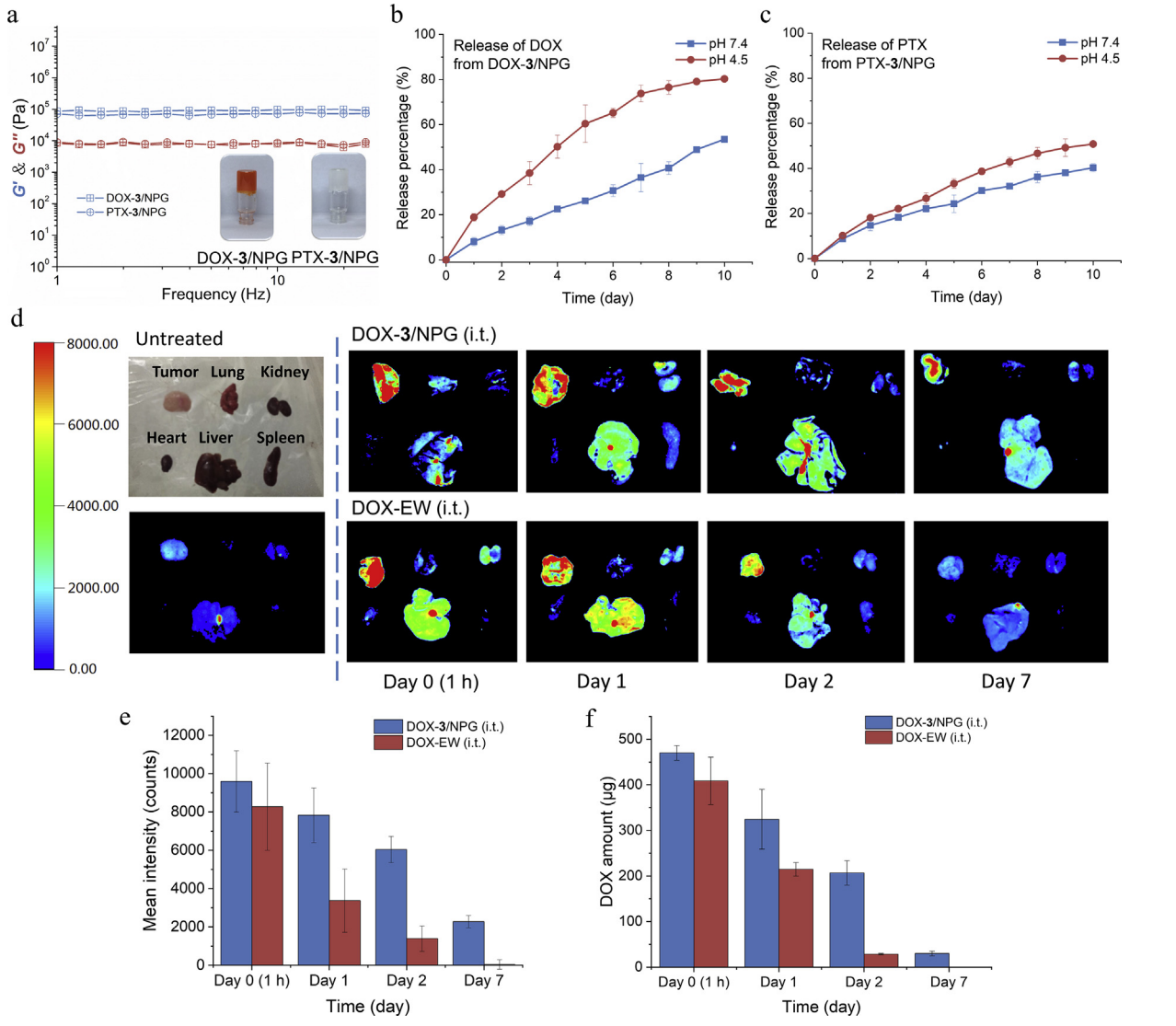

Figure 3 Loading and release of anticancer drugs. (a) Rheological properties of **3**/NPG after drug loading (frequency sweep results for DOX-**3**/NPG (4 mg/mL for DOX, 4 mg/mL for compound **3**, ethanol:water = 1:1) and PTX-**3**/NPG (4 mg/mL for PTX, 4 mg/mL for compound **3**, ethanol:water = 1:1) (photographs are DOX-**3**/NPG and PTX-**3**/NPG, respectively). b) *In vitro* release of DOX at different pH buffers. Data are expressed as mean±SD, $n = 6$. (c) *In vitro* release of PTX at different pH buffers. Error bars, mean±SD, $n = 6$. (d) Visualized *ex vivo* fluorescence imaging of mouse tumors and main organs at different times after treatment, $n = 3$. (e) Fluorescence intensity of DOX in tumor for DOX-**3**/NPG (i.t.) and DOX-EW (i.t.). Data are expressed as mean±SD, $n = 3$. (f) Quantitative analysis of DOX in tumor for DOX-**3**/NPG (i.t.) and DOX-EW (i.t.) by HPLC. Data are expressed as mean±SD, $n = 3$.

a

Group	IC_{50} (μmol/L) for 4T1 murine breast cancer cell	IC_{50} (μmol/L) for MCF-7 human breast cancer cell
Free DOX	11.18	8.11
DOX-GG	10.56	9.01
DOX-**3**/NPG	3.73	2.58
Free PTX	13.78	63.35
PTX-GG	14.60	46.05
PTX-**3**/NPG	2.40	3.20
3/NPG	204.29	748.70

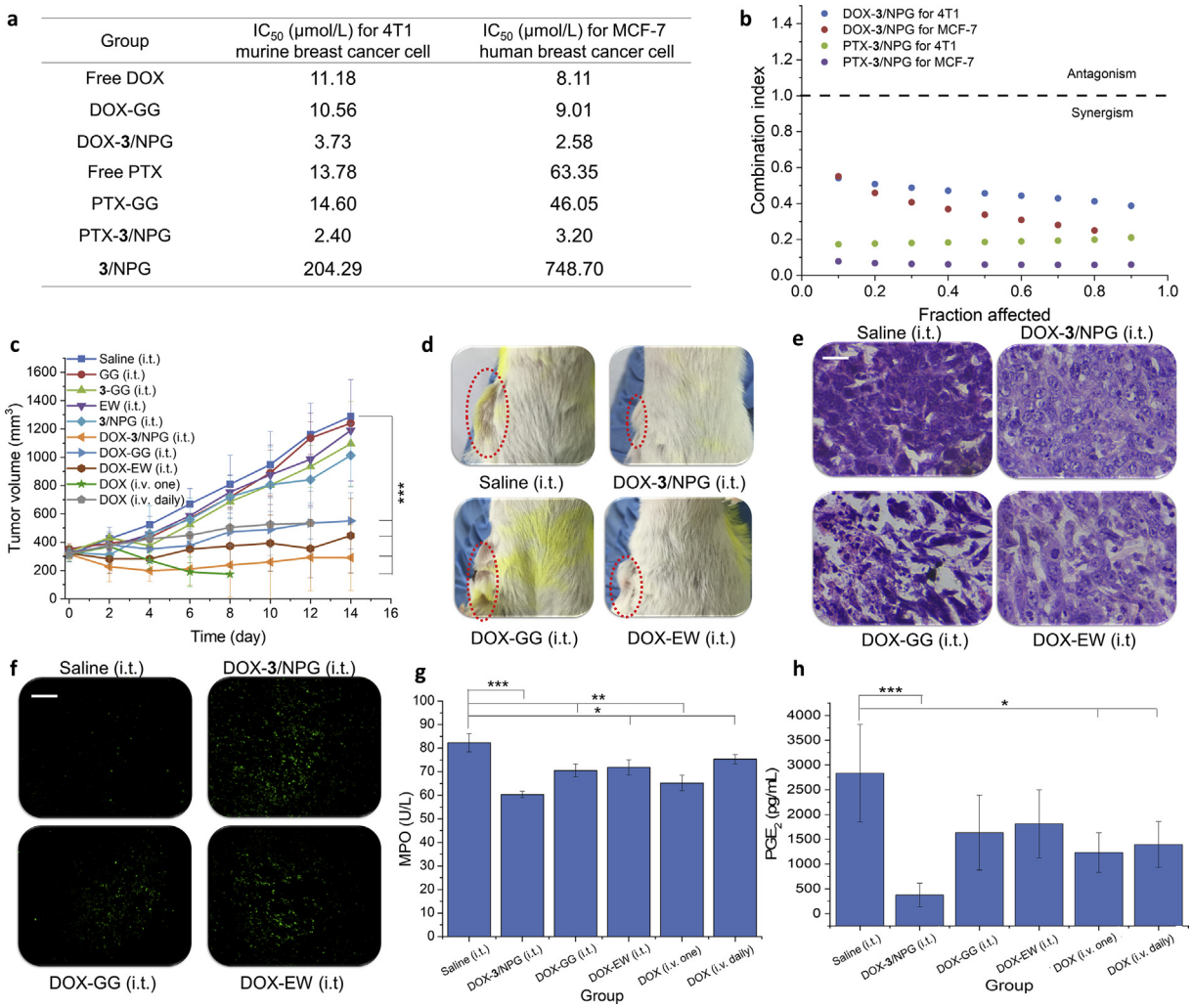

Figure 4 Inhibition of tumor. (a) *In vitro* antitumor activity of drugs-**3**/NPG and drugs-GG against 4T1 murine breast cancer cells and MCF-7 human breast cancer cells (represented by IC_{50} values). (b) Combination index (CI) of drugs-**3**/NPG on 4T1 cells and MCF-7 cells. (c) Changes in tumor volume of tumor-bearing mice after treatment. Data are expressed as mean±SD, $n=8$, $^{***}P<0.001$. (d) Photos of the tumor-bearing sites of mice at 14 days after treatment. (e) H&E staining results of tumors. Scale bars, 100 μm. (f) TUNEL staining results of tumors, magnification 200×. Scale bars, 10 μm. (g) MPO content in mouse serum of DOX-loaded treatment groups. Data are expressed as mean±SD, $n=8$, $^{*}P<0.05$, $^{**}P<0.01$, $^{***}P<0.001$. (h) PGE_2 content in mouse plasma of DOX-loaded treatment groups. Data are expressed as mean±SD, $n=8$, $^{*}P<0.05$, $^{***}P<0.001$.

The *in vivo* anti-inflammatory activity of compounds **1**−**3** was further tested by xylene-induced ear edema in mice. The results showed that the inhibition rate of the compound **3** was the highest (27.7% at 2.0 mg per mouse, $P < 0.001$) (Supporting Information Table S2). Ibuprofen as a reference drug produced an inhibition rate of 25.7% at 0.5 mg per mouse. In view of the above, the NPG constructed from compound **3** (**3**/NPG) was therefore selected as NPG scaffold for treating tumors.

3.3.2. *Loading and release of anticancer drugs*

The hydrophilic antitumor drug DOX and the hydrophobic antitumor drug PTX were selected to verify the ability of NPG scaffold to load different hydrophilic drugs. Due to the two-solvent system of **3**/NPG and excellent self-healing properties, different hydrophilic drugs all can be successfully loaded by incorporation (Fig. 3a), suggesting the drug-loading versatility of NPG scaffold. To assess the possible effects of drug loading on NPG scaffold performance, the rheological properties of **3**/NPG after drug loading were tested. The results showed that the drug-loaded **3**/NPG (drugs-**3**/NPG) still have excellent self-healing properties and almost constant mechanical properties, whether loaded with DOX or PTX (Fig. 3a), indicating that drug loading does not affect the properties of the NPG scaffold.

In vitro drug release showed that the sustained release of the drug in the drugs-**3**/NPG was maintained for at least 10 days and both drugs had a faster release in an acidic environment (Fig. 3b and c). This acid-dependent release is beneficial for the treatment of tumors because the extracellular environment of solid tumors is weakly acidic (pH < 7)[36].

In vivo storage and release of drugs from drugs-**3**/NPG was investigated by anatomy as well as *ex vivo* imaging techniques. Due to the more readily detectable fluorescent properties of DOX, DOX-loaded **3**/NPG (DOX-**3**/NPG) was selected for further study. As a comparison of the **3**/NPG scaffold, a mixed solution of ethanol and water of DOX (DOX-EW) without compound **3** was also tested. The anatomical results showed that at the same time,

the red color (represents DOX) of the tumor site in DOX-**3**/NPG group was always deeper than that of the DOX-EW group, and at 7 days, we could not observe the red color in the DOX-EW group (Supporting Information Fig. S3). *Ex vivo* analysis revealed (Fig. 3d) that at 1 h after injection, the DOX in the DOX-**3**/NPG group was mainly concentrated at the tumor, while DOX in the DOX-EW group was concentrated not only in the tumor but also in the liver. As the monitoring time continued, the DOX signal was decreasing in both groups, but the DOX-**3**/NPG group decreased more slowly. At day 7, no DOX signal was detected in the DOX-EW group, but the DOX signal was still clearly observed in the DOX-**3**/NPG group, indicating that the DOX-**3**/NPG group achieved long-term storage and sustained release at the tumor site. Quantitative analysis of fluorescence signals showed that the intensity of DOX in DOX-**3**/NPG group at day 7 (2276) was actually higher than that in the DOX-EW group at day 2 (1392, Fig. 3e). This suggests that DOX-**3**/NPG can always be stored at a high concentration in the tumor site. Further analysis of the DOX content in the tumor by HPLC showed consistent results with the DOX fluorescence signal (Fig. 3f). The long-term storage and sustained release provided by **3**/NPG are attributed to the encapsulation of DOX by **3**/NPG, which effectively slows the diffuse of DOX, thereby reducing the toxic side effects of the DOX on surrounding tissues and making DOX at a higher drug concentration to effectively kill cancer cells. In DOX-EW, due to the absence of such encapsulation, DOX will diffuse to the surrounding tissues and be rapidly cleared through blood circulation[17], thus losing the above effects.

3.3.3. *In vitro antitumor activity*

The *in vitro* antitumor activity of drugs-**3**/NPG against 4T1 murine breast cancer cells and MCF-7 human breast cancer cells showed that drugs-**3**/NPG increased the antitumor activity of the free drug by 3−20 fold (compared with IC_{50} values, Fig. 4a and Supporting Information Fig. S4). This suggests that the combination of **3**/NPG and whether hydrophobic or hydrophilic drugs can effectively increase the antitumor activity of free drugs. However, no increase in this antitumor activity was observed in the DOX-GG group. We then calculated the combination index (CI) values of drugs and **3**/NPG based on the CI theorem of Chou-Talalay[37]. The results showed that all CI values are less than 1 (Fig. 4b). That is, the enhanced antitumor activities are provided by the synergistic action of the drugs and **3**/NPG.

3.3.4. *In vivo tumor inhibition*

BALB/c mice bearing 4T1 tumors were used to verify the efficacy of *in situ* treatment with DOX-**3**/NPG (intratumoral, i.t.). As a control for the anti-inflammatory active **3**/NPG scaffold, DOX-loaded glycerol gelatin (DOX-GG (i.t.)) was also performed. Glycerol gelatin is commonly used as gel scaffold in drug delivery systems to load hydrophilic or hydrophobic drugs and does not have anti-inflammatory activity[38]. In addition, intratumoral injected DOX-EW (i.t.) as a non-gel scaffold control and intravenously (i.v.) injected DOX physiological saline solution (including one injection group DOX (i.v. one) and daily injection group DOX (i.v. daily)) as a different administration control were also carried out.

From the tumor inhibition results, it was first observed that the tumor inhibition of the DOX-**3**/NPG (i.t.) group was the best (inhibition rate was 97.6%, Fig. 4c) on the 14th day after treatment, that is, the tumor in this group basically no longer grow after treatment. Macroscopic observation revealed that the tumor mass in DOX-**3**/NPG (i.t.) group was also minimal (Fig. 4d). Compared with the DOX-GG (i.t.) group (same dosage form, same administration but no anti-inflammatory activity, inhibition rate was 75.5%), the DOX-**3**/NPG (i.t.) group increased the tumor inhibition rate by 22.1%. This demonstrated that anti-inflammatory activity NPG scaffold provide better tumor inhibition. Secondly, it was observed that other DOX-loaded treatment groups also showed effective inhibition of tumors ($P < 0.001$). However, in the i.v. injected groups (including DOX (i.v. one) and DOX (i.v. daily) group), the mice all died within 12 days after treatment due to serious toxic side effects caused by intravenous administration of chemotherapeutic drugs. In DOX-EW (i.t.) group, although *in situ* administration reduces the systemic toxicity of DOX, DOX still rapidly diffuses into the surrounding tissue due to the absence of the gel encapsulation in DOX-EW. This resulted in a severe ascites reaction and the mice died in the 15th day after treatment (Supporting Information Fig. S5).

H&E staining was used to detect necrosis of cells in tumor tissues. The results showed that in all DOX-loaded treatment groups, a large amount of necrosis occurred in the tumor tissue, mainly in the form of nuclear pyknosis, dissolution and fragmentation (Fig. 4e, all results are shown in Supporting Information Fig. S6). This indicated that the DOX-loaded treatment groups achieved good tumor inhibition by causing cell necrosis. No obvious tumor cell necrosis was observed in the treatment group without DOX loading (Fig. S6).

TUNEL staining was used to detect apoptosis of cells in tumor tissues (green fluorescence represents apoptotic cells). The results showed that the strongest green fluorescence is still in DOX-**3**/NPG (i.t.) group (Fig. 4f, all results are shown in Supporting Information Fig. S7), suggesting that DOX-**3**/NPG has the strongest ability to induce tumor cell apoptosis. Quantitative analysis of the fluorescence intensity of apoptotic cells also confirmed the above observation (Supporting Information Table S3). The analysis showed that the fluorescence intensity of the DOX-**3**/NPG (i.t.) group was the strongest (123,039 ± 8996), which was 3.2 times that of the DOX-GG (i.t.) (38,420 ± 1390) group. This is consistent with the best tumor inhibition of the DOX-**3**/NPG (i.t.) group when monitoring tumor volume.

Taken together, it can be seen that DOX-**3**/NPG constructed from anti-inflammatory active NPG has the best inhibitory effect on tumors in all treatment groups. The best tumor inhibition is not only reflected in its optimal inhibition of tumor growth, but also in its ability to induce apoptosis most strongly.

By comparing with the DOX-GG (i.t.) group, we can preliminarily speculate that the optimal tumor inhibition of DOX-**3**/NPG should be provided by the anti-inflammatory activity of **3**/NPG scaffold. We know that anti-inflammatory active substances improve the therapeutic effect of tumors by altering and regulating the inflammatory mediators and related enzymes in the body. To confirm that optimal tumor inhibition of DOX-**3**/NPG is provided by its anti-inflammatory activity, we first tested myeloperoxidase (MPO) in the blood of tumor-bearing mice (its inhibition is an indicator for evaluating the anti-inflammatory activity of a substance)[39]. The results showed that MPO levels in all DOX-loaded treatment groups were reduced compared to the saline (i.t.) group (Fig. 4g). In comparison, however, the reduction in MPO in DOX-**3**/NPG (i.t.) group was still the highest (reaching 36%), demonstrating that DOX-**3**/NPG has the

strongest anti-inflammatory activity. We then determined prostaglandin E_2 (PGE_2) in the blood of tumor-bearing mice, which is considered to be the most relevant and important prostaglandin for inflammation[40]. Furthermore, the study of PGE_2 in the field of tumors have revealed that PGE_2 is highly expressed in different tumor tissues, and it is generally believed that high expression of PGE_2 can mediate different signal transduction pathways to promote tumor cell survival and anti-apoptotic processes[41,42]. The PGE_2 content results showed that all DOX-loaded treatment groups had a lower PGE_2 levels than the saline (i.t.) group (Fig. 4h). However, the proportion of PGE_2 reduction in DOX-**3**/NPG (i.t.) group was still the largest, reaching 652%. Therefore, we speculate that compound **3**, as an anti-inflammatory natural product with a similar structure to steroidal anti-inflammatory drugs, first reduces PGE_2 content by decreasing the expression of cyclooxygenase 2[43] Thereafter, the decrease of PGE_2 content will further negatively regulate the survival, proliferation and anti-apoptosis of tumor cells, which produces the best anti-tumor effect of DOX-**3**/NPG.

*3.3.5. Other advantages of DOX-**3**/NPG in treating tumors*

In addition to optimal inhibition of tumors, DOX-**3**/NPG exhibits superior therapeutic effects over other treatment groups in a variety of aspects including health status, body recovery, immune function, side effects and survival.

Improvement of health: the overall health of the mice was assessed by monitoring blood routine because it sensitively reflects the pathological changes of the body. White blood cells (WBC), red blood cells (RBC) and platelets (PLT) are the most diagnostic reference values in routine blood test. Therefore, we dynamically monitored routine blood data of tumor-bearing mice throughout the course of treatment (days 0, 7, and 14). Routine blood data of normal mice (tumor-free mice, normal group) was tested and used as a reference. In the WBC results (Fig. 5a), an increase in WBC was observed in all groups, which was caused by inflammation caused by the tumor. Especially in the saline, GG, **3**-GG, and EW groups, WBC increased more due to the lack of drug DOX for tumor treatment. In all DOX-loaded treatment groups, the amount of WBC in the DOX-**3**/NPG group

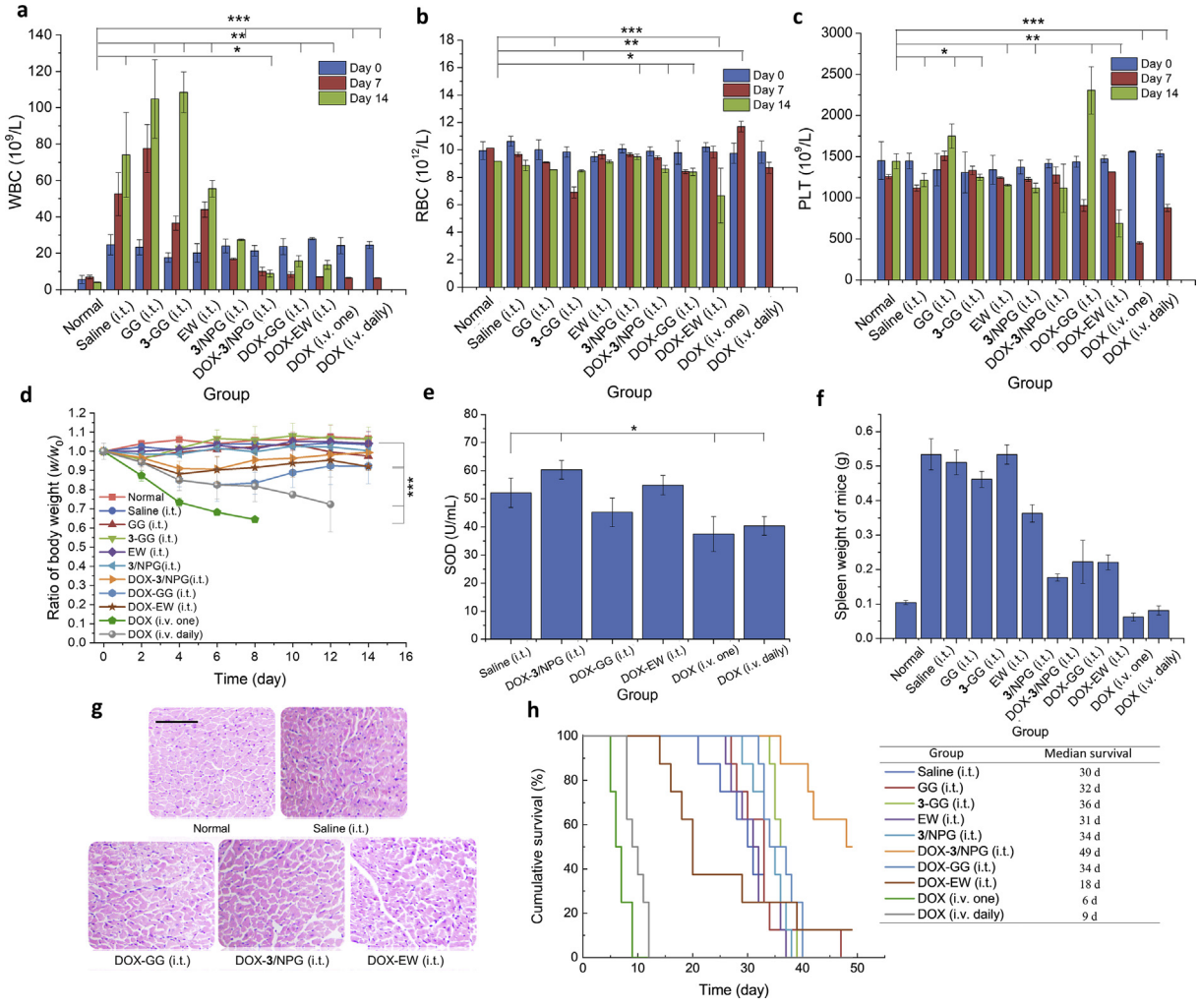

Figure 5 Other advantages of DOX-**3**/NPG in treating tumors. (a) WBC in routine blood test, $^{*}P<0.05$, $^{**}P<0.01$, $^{***}P<0.001$. Data are expressed as mean±SD, $n=8$. (b) RBC in routine blood test, $^{*}P<0.05$, $^{**}P<0.01$, $^{***}P<0.001$. Data are expressed as mean±SD, $n=8$. (c) PLT in routine blood test, $^{*}P<0.05$, $^{**}P<0.01$, $^{***}P<0.001$. Data are expressed as mean±SD, $n=8$. (d) Changes in body weight of tumor-bearing mice after treatment. Data are expressed as mean±SD, $n=8$, $^{***}P<0.001$. (e) SOD content in mouse serum. Data are expressed as mean±SD, $n=8$, $^{*}P<0.05$. (f) Spleen weight of mice. Data are expressed as mean±SD, $n=8$. (g) H&E staining results of hearts. Scale bars, 100 μm. (h) Survival time and median survival of tumor-bearing mice. $n=8$.

was closest to that in the normal group, suggesting that inflammation in the DOX-**3**/NPG group was minimal. In the RBC results (Fig. 5b), the RBC of the mice in each group showed different degrees of fluctuation, and the fluctuations in the DOX-**3**/NPG (i.t.) group were still the smallest. In the PLT results (Fig. 5c), there was a significant increase in PLT in the GG and the DOX-GG group, which may be a manifestation of chronic inflammation produced by the presence of glycerol. In the DOX (i.v. one) and DOX (i.v. daily) group, PLT showed a significant decrease due to the toxic side effects of intravenous injection of DOX. In comparison, the DOX-**3**/NPG (i.t.) group still maintains a relatively normal state, and PLT data were not significantly different from the normal group. The above results showed that the mice in DOX-**3**/NPG (i.t.) group had the closest indicator to the normal group. That is, mice in the DOX-**3**/NPG (i.t.) group have the healthiest state throughout the treatment.

Acceleration of body recovery: body weight and SOD content were measured to evaluate the recovery status of the mice. Body weight result revealed that the mice in all DOX-loaded treatment groups showing significant weight loss after treatment (Fig. 5d). However, in the following time, only the DOX-**3**/NPG (i.t.), DOX-EW (i.t.) and DOX-GG (i.t.) groups began to gradually increase in body weight. Among them, the DOX-**3**/NPG (i.t.) group had the fastest weight gain, and there was no significant difference from the normal group on the 14th day. This indirectly reflects the fact that the DOX-**3**/NPG can return the mouse body to normal more quickly. However, the body weight of mice in DOX (i.v. one) and DOX (i.v. daily) groups continued to decline until all died. SOD specifically removes harmful free radicals from the body to recover normal body function as quickly as possible[44]. Although SOD is a non-specific auxiliary diagnostic index, it has important reference value for the evaluation of the body's recover after treatment. The measurement of SOD in the blood of mice showed that only the DOX-**3**/NPG (i.t.) and the DOX-EW (i.t.) groups had higher SOD content than the saline (i.t.) group (Fig. 5e). Among them, the increase in DOX-**3**/NPG (i.t.) group was still the highest, which was higher than 14% of the SOD content in saline (i.t.) ($P < 0.05$). This suggests that mice in DOX-**3**/NPG (i.t.) group have better body recovery conditions than other treatment groups.

Enhancement of immune function: the spleen is the largest peripheral immune organ. Usually, the spleen enlargement helps to improve the body's immunity. However, during tumor development, excessive spleen enlargement can shift the function of the spleen from positive to negative immunomodulation, which in turn promotes tumor growth[45]. To examine changes in immune function after treatment, the spleen changes in mice were measured. The results showed that except for the DOX (i.v. one) and DOX (i.v. daily) groups (the damage produced by intravenous administration of DOX in both groups causes the spleen to become smaller, that is, the immune system is destroyed), the spleens of the other treatment groups showed different degrees of increase (the increase range was 1.70−5.12 times that of the normal mice) (Fig. 5f). If we define that the spleen is doubled, it is excessively enlarged. It can be seen that in all treatment groups, only the spleen in DOX-**3**/NPG (i.t.) group was normally enlarged (1.70 times), that is, only the spleens in this group still exerted a positive immunomodulatory.

Reduction of chemotherapeutic cardiotoxicity: as a non-specific anti-tumor drug, the serious cardiotoxicity of the DOX is an important reason for limiting its clinical application[46,47]. H&E staining of the heart was used to evaluate the cardiotoxicity of DOX in different treatment groups (Fig. 5g and Supporting Information Fig. S8). The heart of the mice in normal group served as a reference for the normal heart. The results showed that DOX damage to the heart was observed in all DOX-loaded treatment groups, mainly reflecting in the disordered, loose, and irregular morphology of cardiomyocytes in varying degrees. However, in comparison, the heart in the DOX-**3**/NPG (i.t.) group still showed a morphology closer to that of normal mice, such as neatly aligned cells, relatively intact morphology, and well-defined nuclei. This suggests that DOX-**3**/NPG can better reduce the cardiotoxicity caused by DOX. This protection is most likely to be achieved by compound **3** to eliminate free radicals in the body to reduce peroxide-induced damage, thereby reducing DOX toxicity and effectively protecting cardiomyocytes[48].

Prolonged survival: at present, it is extremely difficult to completely cure tumors, thus maximizing the survival of tumor-bearing mice is a key indicator for evaluating the therapeutic effect of tumors. Survival results showed a median survival of 30 days in the saline (i.t.) group, while treatment with DOX-**3**/NPG increased the median survival from 30 to 49 days (that is, prolonging the survival of tumor-bearing mice by 63%) (Fig. 5h). In the other DOX-loaded treatment groups, the longest median survival was only 34 days (*i.e.*, only 20% increase). Far from prolonging the survival of the mice, the treatment of intravenous administration accelerated the death of the mice (the median survival for DOX (i.v. one) and DOX (i.v. daily) groups was only 6 and 9 days, respectively). This actually reflects a very critical issue, that is, the DOX-loaded treatment groups all can produce a good inhibitory effect on the tumor. However, except for the DOX-**3**/NPG (i.t.) group, the other groups were unable to effectively prolong the survival of the mice. This phenomenon has also been observed in other studies in which tumors are treated with *in situ* injectable gel scaffolds constructed with non-pharmacologically active synthetic compounds. For example, the treatment of phenylboronic acid-based *in situ* gel scaffold has a median survival of 36 days in the optimal group and 30 days in the saline group[49]. In another case, the treatment of phospholipid-based *in situ* gel scaffold has a median survival of only 14 days in the optimal group and 9 days in the saline group[50]. In these non-bioactive gel scaffolds, drug-loaded gels were not effective in prolonging the survival of tumor-bearing mice at all. However, the application of the bioactive NPG scaffold can not only effectively inhibit tumor growth, but also maximize the lifespan of tumor-bearing mice under conditions of better body recovery, stronger immune function, less toxic side effects. This embodies the enormous advantages of NPG scaffolds and demonstrates the efficacy of NPG scaffolds in the treatment of disease.

4. Conclusions

Here, we have developed a series of injectable gel scaffolds with different biological activities using self-assembled natural products. Surprisingly, these injectable NPG scaffolds also exhibit the characteristics of an ideal gel scaffolds designed (encompassing excellent self-healing, controlled gelation, good safety, sustained release and biodegradability, biocompatibility, biostability, etc.). The combination of multispectral techniques confirmed that the formation of NPG scaffolds was not only supported by weak non-covalent forces, but also supported by solvent participation. Based on this result, a possible self-assembly process of triterpenoid NPG is proposed, which provides guidance and reference for the formation of triterpenoid NPG. Choosing the appropriate

pharmacologically active NPG scaffold to treat the disease and improving the therapeutic effect are the biggest advantage of applying NPG scaffolds. This advantage has also been fully confirmed in this work. *In vitro* and *in vivo* experiments demonstrated that DOX-**3**/NPG can significantly improve the therapeutic effect on tumors through synergistic action, and this effect is achieved by anti-inflammatory active compound **3** regulating the expression of COX 2 to reduce PGE_2 content. In addition, the anti-inflammatory **3**/NPG scaffold also shows superior efficacy over non-bioactive gel scaffolds in improving health, accelerating body recovery, enhancing immune function, reducing chemotherapeutic cardiotoxicity and prolonging survival. Taken together, the successful construction of injectable NPG scaffolds for drug delivery not only takes advantage of the self-assembled natural products, compensates for the lack of biological activity of the injectable gel scaffolds, but also enables the development of new applications for natural products. As a prospect, in the future, choosing self-assembled natural products with the desired pharmacological activity from a large number of bioactive natural products to construct drug delivery system will certainly make natural products play a greater role in the treatment of more diseases.

Acknowledgments

This work was supported by the National Natural Science Foundation of China, Nos. 31972040 and 31571798, Heilongjiang provincial financial support project (Xin Yang), and Harbin Special Foundation for Excellent Academic Leader Project, No. 2014RFXXJ113, China.

Author contributions

Kangkang Zhi was responsible for conceptualization, methodology, investigation, writing and visualization. Jiacheng Wang were responsible for methodology and investigation. Haitian Zhao was responsible for resources, supervision and funding acquisition. Xin Yang was responsible for conceptualization, resources, writing, supervision and funding acquisition.

Conflicts of interest

The authors have no conflicts of interest to declare.

Appendix A. Supporting information

Supplementary data to this article can be found online at https://doi.org/10.1016/j.apsb.2019.09.009.

References

1. Blunt JW, Copp BR, Keyzers RA, Munro MH, Prinsep MR. Marine natural products. *Nat Prod Rep* 2017;**34**:235−94.
2. Rodrigues T, Reker D, Schneider P, Schneider G. Counting on natural products for drug design. *Nat Chem* 2016;**8**:531−41.
3. Molinski TF. All natural: the renaissance of natural products chemistry. *Org Lett* 2014;**16**:3849−55.
4. Zhi K, Zhao H, Yang X, Zhang H, Wang J, Wang J, et al. Natural product gelators and a general method for obtaining them from organisms. *Nanoscale* 2018;**10**:3639−43.
5. He N, Zhi K, Yang X, Zhao H, Zhang H, Wang J, et al. Self-assembled fibrillar networks induced by two methods: a new unmodified natural product gel. *New J Chem* 2018;**42**:14170−8.
6. Bag BG, Majumdar R. Self-assembly of renewable nano-sized triterpenoids. *Chem Rec* 2017;**17**:841−73.
7. Zhi K, Yang X. Natural product gels and their gelators. *Prog Chem* 2019;**31**:1314−28.
8. Zheng J, Fan R, Wu H, Yao H, Yan Y, Liu J, et al. Directed self-assembly of herbal small molecules into sustained release hydrogels for treating neural inflammation. *Nat Commun* 2019;**10**:1604.
9. Rogers MA, Feng Q, Ladizhansky V, Good DB, Smith AK, Corridini M, et al. Self-assembled fibrillar networks comprised of a naturally-occurring cyclic peptide-LOB3. *RSC Adv* 2016;**6**:40765−76.
10. Bag BG, Majumdar R. Vesicular self-assembly of a natural triterpenoid arjunolic acid in aqueous medium: study of entrapment properties and *in situ* generation of gel-gold nanoparticle hybrid material. *RSC Adv* 2014;**4**:53327−34.
11. Bag BG, Das S, Hasan SN, Barai AC. Nanoarchitectures by hierarchical self-assembly of ursolic acid: entrapment and release of fluorophores including anticancer drug doxorubicin. *RSC Adv* 2017;**7**:18136−43.
12. Ramin MA, Sindhu KR, Appavoo A, Oumzil K, Grinstaff MW, Chassande O, et al. Cation tuning of supramolecular gel properties: a new paradigm for sustained drug delivery. *Adv Mater* 2017;**29**:1605227.
13. Liu Q, Zhan C, Barhoumi A, Wang W, Santamaria C, McAlvin JB, et al. A supramolecular shear-thinning anti-inflammatory steroid hydrogel. *Adv Mater* 2016;**28**:6680−6.
14. Weiss RG. The past, present, and future of molecular gels. What is the status of the field, and where is it going?. *J Am Chem Soc* 2014;**136**:7519−30.
15. Ishii S, Kaneko J, Nagasaki Y. Development of a long-acting, protein-loaded, redox-active, injectable gel formed by a polyion complex for local protein therapeutics. *Biomaterials* 2016;**84**:210−8.
16. Ramin MA, Latxague L, Sindhu KR, Chassande O, Barthélémy P. Low molecular weight hydrogels derived from urea based-bolaamphiphiles as new injectable biomaterials. *Biomaterials* 2017;**145**:72−80.
17. Kim DY, Kwon DY, Kwon JS, Park JH, Park SH, Oh HJ, et al. Synergistic anti-tumor activity through combinational intratumoral injection of an *in-situ* injectable drug depot. *Biomaterials* 2016;**85**:232−45.
18. Hill RA, Connolly JD. Triterpenoids. *Nat Prod Rep* 2018;**35**:1294−329.
19. Tai T, Akahori A, Shingu T. Triterpenoids from *Poria cocos*. *Phytochemistry* 1991;**30**:2796−7.
20. Tai T, Shingu T, Kikuchi T, Tezuka Y, Akahori A. Triterpenes from the surface layer of *Poria cocos*. *Phytochemistry* 1995;**39**:1165−9.
21. Carpenter RC, Sotheeswaran S, Sultanbawa MU, Ternai B. ^{13}C NMR studies of some lupane and taraxerane triterpenes. *Org Magn Reson* 1980;**14**:462−5.
22. Tseng JC, Kung AL. *In vivo* imaging method to distinguish acute and chronic inflammation. *J Vis Exp* 2013;**2013**:e50690.
23. Cho JY, Park J, Yoo ES, Baik KU, Jung JH, Lee J, et al. Inhibitory effect of sesquiterpene lactones from *Saussurea lappa* on tumor necrosis factor-α production in murine macrophage-like cells. *Planta Med* 1998;**64**:594−7.
24. Vogel HG, Vogel WH. *Drug discovery and evaluation: pharmacological assays*. Berlin: Springer; 2013.
25. Akihisa T, Uchiyama E, Kikuchi T, Tokuda H, Suzuki T, Kimura Y. Anti-tumor-promoting effects of 25-methoxyporicoic acid A and other triterpene acids from *Poria cocos*. *J Nat Prod* 2009;**72**:1786−92.
26. Symon AV, Veselova NN, Kaplun AP, Vlasenkova NK, Fedorova GA, Lyutik AI, et al. Synthesis and antitumor activity of cyclopropane derivatives of betulinic and betulonic acids. *Russ J Bioorganic Chem* 2005;**31**:286−91.
27. Kikuchi T, Uchiyama E, Ukiya M, Tabata K, Kimura Y, Suzuki T, et al. Cytotoxic and apoptosis-inducing activities of triterpene acids from *Poria cocos*. *J Nat Prod* 2011;**74**:137−44.

28. Pavlova NI, Savinova OV, Nikolaeva SN, Boreko EI, Flekhter OB. Antiviral activity of betulin, betulinic and betulonic acids against some enveloped and non-enveloped viruses. *Fitoterapia* 2003;**74**:489−92.
29. Yu G, Yan X, Han C, Huang F. Characterization of supramolecular gels. *Chem Soc Rev* 2013;**42**:6697−722.
30. Cheng T, Zhao Y, Li X, Lin F, Xu Y, Zhang X, et al. Computation of octanol−water partition coefficients by guiding an additive model with knowledge. *J Chem Inf Model* 2007;**47**:2140−8.
31. Silverstein RM, Webster FX, Kiemle DJ, Bryce DL. *Spectrometric identification of organic compounds*. 8th ed. New York: Wiley; 2014.
32. Worsfold P, Townshend A, Poole C. *Encyclopedia of analytical sciences*. London: Academic Press; 2004.
33. Grivennikov SI, Greten FR, Karin M. Immunity, inflammation, and cancer. *Cell* 2010;**140**:883−99.
34. Aggarwal BB, Vijayalekshmi RV, Sung B. Targeting inflammatory pathways for prevention and therapy of cancer: short-term friend, long-term foe. *Clin Cancer Res* 2009;**15**:425−30.
35. Cho JY, Baik KU, Jung JH, Park MH. *In vitro* anti-inflammatory effects of cynaropicrin, a sesquiterpene lactone, from *Saussurea lappa*. *Eur J Pharmacol* 2000;**398**:399−407.
36. Zhang L, Xia J, Zhao Q, Liu L, Zhang Z. Functional graphene oxide as a nanocarrier for controlled loading and targeted delivery of mixed anticancer drugs. *Small* 2010;**6**:537−44.
37. Chou TC. Theoretical basis, experimental design, and computerized simulation of synergism and antagonism in drug combination studies. *Pharmacol Rev* 2006;**58**:621−81.
38. Rowe RC, Sheskey PJ, Quinn ME. *Handbook of pharmaceutical excipients*. 6th ed. London: Pharmaceutical Press; 2009.
39. Bradley PP, Priebat DA, Christensen RD, Rothstein G. Measurement of cutaneous inflammation: estimation of neutrophil content with an enzyme marker. *J Investig Dermatol* 1982;**78**:206−9.
40. Yuhki KI, Ueno A, Naraba H, Kojima F, Ushikubi F, Narumiya S, et al. Prostaglandin receptors EP2, EP3, and IP mediate exudate formation in carrageenin-induced mouse pleurisy. *J Pharmacol Exp Ther* 2004;**311**:1218−24.
41. Rahman MA, Dhar DK, Yamaguchi E, Maruyama S, Sato T, Hayashi H, et al. Coexpression of inducible nitric oxide synthase and COX-2 in hepatocellular carcinoma and surrounding liver: possible involvement of COX-2 in the angiogenesis of hepatitis C virus-positive cases. *Clin Cancer Res* 2001;**7**:1325−32.
42. Castellone MD, Teramoto H, Williams BO, Druey KM, Gutkind JS. Prostaglandin E_2 promotes colon cancer cell growth through a G_s-axin-β-catenin signaling axis. *Science* 2005;**310**:1504−10.
43. Katzung BG, Masters SB, Trevor AJ. *Basic & clinical pharmacology*. 12th ed. New York: McGraw-Hill Companies; 2012.
44. Howard MD, Greineder CF, Hood ED, Muzykantov VR. Endothelial targeting of liposomes encapsulating SOD/catalase mimetic EUK-134 alleviates acute pulmonary inflammation. *J Control Release* 2014;**177**:34−41.
45. Brar SS, Seevaratnam R, Cardoso R, Law C, Helyer L, Coburn N. A systematic review of spleen and pancreas preservation in extended lymphadenectomy for gastric cancer. *Gastric Cancer* 2012;**15**:89−99.
46. Minotti G, Cavaliere AF, Mordente A, Rossi M, Schiavello R, Zamparelli R, et al. Secondary alcohol metabolites mediate iron delocalization in cytosolic fractions of myocardial biopsies exposed to anticancer anthracyclines. Novel linkage between anthracycline metabolism and iron-induced cardiotoxicity. *J Clin Investig* 1995;**95**:1595−605.
47. Minotti G, Menna P, Salvatorelli E, Cairo G, Gianni L. Anthracyclines: molecular advances and pharmacologic developments in antitumor activity and cardiotoxicity. *Pharmacol Rev* 2004;**56**:185−229.
48. Gilleron M, Marechal X, Montaigne D, Franczak J, Neviere R, Lancel S. NADPH oxidases participate to doxorubicin-induced cardiac myocyte apoptosis. *Biochem Biophys Res Commun* 2009;**388**:727−31.
49. Gao W, Liang Y, Peng X, Hu Y, Zhang L, Wu H, et al. *In situ* injection of phenylboronic acid based low molecular weight gels for efficient chemotherapy. *Biomaterials* 2016;**105**:1−11.
50. Wu W, Chen H, Shan F, Zhou J, Sun X, Zhang L, et al. A novel doxorubicin-loaded *in situ* forming gel based high concentration of phospholipid for intratumoral drug delivery. *Mol Pharm* 2014;**11**:3378−85.